ORIGINAL RESEARCH PAPER

Synthesis, Characterization and Photocatalytic study of FeCr$_2$O$_4$@ZnO@MgO Core-Shell Nanoparticle

Borhade Ashok. V, Tope Dipak. R, Agashe Jyoti. A, Kushare Sachin. S

Research Centre, Department of Chemistry, HPT Arts and RYK Science College, Nashik 422005, Maharashtra, India. Affiliated to Savitribai Phule Pune University, Pune-411007, Maharashtra, India

ABSTRACT

In the present work, the sol-gel derived powders of the chemical form FeCr$_2$O$_4$@ZnO@MgO core-shell, have been synthesized and used as a photocatalyst. The synthesized core-shell nanoparticles are characterized by various analytical techniques including FTIR, XRD, SEM-EDAX, and HR-TEM-SEAD. The successful performance of synthesized core-shell photocatalyst FeCr$_2$O$_4$@ZnO@MgO has been also demonstrated for the complete mineralization of Orange G dye. The effect of various operational parameters used in dye degradation such as concentration of dye, light intensity, amount of photocatalyst, the effect of light, and effect of electrolyte has been studied on the rate of reaction. TEM analysis clearly shows two layers of ZnO and MgO on FeCr$_2$O$_4$. The highest degradation rate was found with the concentration of Orange G dye 10 ppm, 0.8 g of FeCr$_2$O$_4$@ZnO@MgO, and time 50 min. The recyclability of the photocatalyst, FeCr$_2$O$_4$@ZnO@MgO was performed up to four runs. The degradation mechanism has been established by using LC-MS analysis and it was used to track the numerous intermediate products formed during Orange G dye degradation.

Keywords: *Sol-gel, Photocatalytic degradation, Orange G dye, LC-MS.*

INTRODUCTION

Water pollution has become a major worldwide problem due to rapid industrial growth. Apart from various aqueous pollutants, hazardous metal ions and dyes have provoked increasing public contact due to their wide use in many industries including pharmaceutical, printing, textile, food, and leather industry. The report in literature reveals that a large amount of dyes (nearly 20%) of worldwide production is discharged by textile factories because of incomplete exhaustion of coloring materials and washing operations [1,2]. Further, it is also reported that a large number of dyes and their metabolites have been reported to be hazardous, toxic, mutagenic, and carcinogenic [3,4].

The high concentration of organics in the effluents and the stability of modern synthetic dyes make the conventional biological methods for wastewater treatment ineffective for the complete color removal and degradation of organic pollutants [5,6]. Environmental pollution has been increasing and steps towards the development of low-cost materials to overcome these problems have gained importance [7-10]. Besides this, some dyes in particular form can undergo anaerobic decoloration to potentially carcinogenic amines [11]. Consequently, there is a considerable need to treat these colored effluents before discharging them to various water bodies. Advanced oxidation

* Corresponding Author Email: *ashokborhade2007@yahoo.co.in*
                              sachinkushare7@gmail.com

processes (AOP's) employing heterogeneous catalysts have emerged as potentially destructive technologies leading to the complete removal of most organic pollutants [12-14]. In tropical countries like India, where an ample amount of sunlight is available, photocatalysis involving sunlight will be economical and preferable, unlike other energy-intensive irradiation sources. Among the various semiconductors employed, TiO$_2$ and ZnO are well-known photocatalysts for the degradation of several environmental contaminants due to their high photosensitivity, stability, and large bandgap [15-20]. Hence, it is essential to develop an effective photocatalyst for the degradation of organic pollutants under sunlight/visible light irradiation. Heterogeneous photocatalysis employing aqueous suspension of ZnO through the illumination of sunlight is relatively significant among the AOP removal of textile dyes from wastewater because of its mild operating conditions [21]. The photocatalytic efficiency of semiconductor metal oxide in the presence of visible irradiation has been reported in the literature for the degradation of organic dyes [22-24]. Core-shell multifunctional magnetic nanoparticles have a wide variety of applications including catalysis, magnetic separation, and numerous biomedical uses [25-28]. By contrast, GeO$_2$ is a dielectric semiconductor oxide with a broadband (~3.4 eV) [29], which has high catalytic activity in the ultraviolet region (λ< 350 nm).

The present work focuses on the preparation and investigation of iron (II) chromite-based nanoparticles which are coated by ZnO and MgO forming core-shell FeCr$_2$O$_4$@ZnO@MgO. The application of a ZnO coating layer between iron (II) chromite and MgO may reduce the recombination process between MgO and iron (II) chromite. The goal of the present work is to test this new FeCr$_2$O$_4$@ZnO@MgO core-shell nanostructures as photocatalysts for the photo-oxidation of Orange G dye, under UV light and evaluate their potential as magnetically retrievable and re-usable photocatalysts. The iron (II) chromite core material was selected because it is more thermally stable for the preparation of core-shell. This particular dye was chosen because it has a variety of functional groups such as the sulfonate, aryl, hydroxyl, and azo groups. The degraded products were analyzed by LC-MS and intermediate products formed are separated and characterized. LC-MS study enabled us to establish the mechanistic pathway for degradation of Orange G dye.

METHODS AND MATERIALS
Materials

The FeCr$_2$O$_4$, FeCr$_2$O$_4$@ZnO, and FeCr$_2$O$_4$@ZnO@MgO core-shell nanoparticles were prepared from the chemicals without further purification. The chemicals used are Ferric nitrate Fe(NO$_3$)$_3$.6H$_2$O, Chromium nitrate Cr(NO$_3$)$_3$.9H$_2$O, Zinc nitrate Zn(NO$_3$)$_2$.6H$_2$O, Magnesium nitrate Mg(NO$_3$)$_2$.6H$_2$O, Triton-X-100, and Orange G dye analytical grade were purchased from Sigma-Aldrich.

EXPERIMENTAL
Synthesis of FeCr$_2$O$_4$ Nanoparticles

The nanoparticle FeCr$_2$O$_4$ was synthesized by the sol-gel method using Ferric nitrate Fe(NO$_3$)$_3$.9H$_2$O (1 M) and Chromium nitrate Cr(NO$_3$)$_3$.6H$_2$O (2 M) as precursors and Triton X-100 was dissolved in 100 ml double distilled water. NaOH solution (1.5 M) was slowly dropped under vigorous stirring to obtain a precipitate solution with a pH of 12. The solution was transferred in a Steel lined Teflon autoclave and kept at 121 ^{0}C for a period of 24 hrs in the oven. The resultant gel was filtered and repeatedly washed with double distilled water. Subsequently, the washed precipitate was dried at 110 ^{0}C for 6 hrs and calcined at 800 ^{0}C for another 4 hrs.

Synthesis of FeCr$_2$O$_4$@ZnO Core-Shell Nanoparticles

The ZnO coating was performed by dissolving, FeCr$_2$O$_4$ (1 M) and Zinc nitrate Zn (NO$_3$)$_3$.9H$_2$O (2 M) in 100 ml double distilled water. Further NaOH solution (1 M) was added dropwise under vigorous stirring for 1 hour to obtain a precipitate. The slurry obtained was refluxed at 120 ^{0}C for 24 hrs. The precipitate was washed by using double distilled water and dried at 110 ^{0}C for 2 hrs, then calcined at 850 ^{0}C for 6 hrs to remove organic matter.

Synthesis of FeCr$_2$O$_4$@ZnO@MgO Core-Shell Nanoparticles

The FeCr$_2$O$_4$@ZnO@MgO Core-Shell Nanoparticles were prepared by dissolving FeCr$_2$O$_4$@ZnO (1 M) and Magnesium nitrate Mg (NO$_3$)$_3$.9H$_2$O (2 M) into 100 ml NaOH (1 M) solution under vigorous shaking. Then obtained material was stirred for 2 hrs and kept in a steel-lined Teflon autoclave in the oven at 121 ^{0}C for

J. Water Environ. Nanotechnol., 6(2): 164-176 Spring 2021

165

24 hrs. When the reaction was completed, the precipitate obtained was filtered and washed with deionized water, and dried at 110 °C for 6 hrs. The dried product was ground in mortar- pestle to prepare fine powder. The resulting brown polycrystalline product was heated at 900 °C for 6 hrs in a muffle furnace.

CHARACTERIZATION

All synthesized nanoparticles were characterized by appropriate analytical techniques including FTIR, XRD, SEM–EDAX, and HR-TEM-SEAD analysis. IR study (KBr pellets) was performed on a Shimadzu 8400S FTIR spectrometer in the range of 4000 to 400 cm^{-1}. The phase purity of the product was confirmed by X-ray powder diffraction pattern using Rigaku Ultima IV copper instrument operating at 25 kV and 25 mA using Ka radiation with wavelength k = 0.154 nm. SEM–EDAX analysis was carried by scanning electron microscope JEOL-6390LA equipment, transmission electron microscope (HRTEM-JEOL/JEM 2100, operating voltages 200kV, LaB6 Electron gun, Point resolution 0.23 nm Lattice resolution 0.14 nm) instrument.

PHOTOCATALYSIS

In the current work, the photodegradation of Orange G dye was concentrated by utilizing Synthesized Core-Shell nanoparticles. Four kinds of perception were recorded. In the principal test, 50 ml 10 ppm solution of Orange G dye was irradiated in a photoreactor utilizing 0.8 g of FeCr$_2$O$_4$@ZnO@MgO Core-Shell nanoparticles as a photocatalyst. The subsequent trial was completed without light. In the third test, just Orange G dye solution without catalyst was irradiated with UV–visible light in a photoreactor. The fourth examination was done without light without Catalyst. The abatement in absorbance because of mineralization of Orange G dye was recorded on a double-beam UV–visible spectrophotometer (Systronic) after each 10 min.

HPLC–MS ANALYSIS OF ORANGE G DYE-DEGRADED SOLUTION

The chromatographic trials with HPLC–UV–visible framework were done on HPLC (Water, 840) utilizing water a Nestgroup C-18 reverse-phase section (2 by 25 cm). The samples were eluted with a linear gradient of (CH$_3$)$_2$CO/H$_2$O 45/55% to 90/10%. The slope elution was from 5 to 90% in 30 min, the stream rate was 0.5 ml/min and

the injection volume was 100 μl. The peaks were observed at 475 nm with a detection range between 220 and 680 nm. The slope HPLC partition was combined with an ion trap mass spectrometer (water). The mass spectrometer was outfitted with electrospray ionization sources and operated in positive polarity. The mass reach was from 50 to 500 m/z. Tandem mass analysis was finished utilizing the auto mass mode, where helium gas was utilized as collision gas.

RESULTS AND DISCUSSION

FT-IR Spectroscopy

The FTIR analysis, as the main reference, was used to study the molecular structure, demonstrating each stretching mode in nanoparticles, as presented in Fig 1. The FTIR spectrum of nanoparticles was analyzed in the range of 400–4000 cm^{-1}. The peaks in Fig.1(a) located at 3450 cm^{-1} correspond to the O-H stretching functional group. Nonetheless, the OH bending functional group is shown at 1650 cm^{-1}. Also, the peaks at 950 cm^{-1} correspond to the C-H bending functional group. Transmission peaks at 700 and 418 cm^{-1} correspond to spectra that have tetrahedral and octahedral oxygen-metal M-O bonds. This range shows the characteristics of atomic vibrations in the tetrahedral and octahedral positions in the cubic structure [30]. Fig.1(b) shows synthesized FeCr$_2$O$_4$@ZnO nanoparticles. Peaks at 3353.65 and 3440.43 cm^{-1} represent the bending vibration of H$_2$O and the presence of OH stretching in ZnO. Peaks in the range of 400–600 cm^{-1} represent the characteristic metal-oxygen (M–O) vibrational modes.

The peak at 470 cm^{-1} indicates the development of ZnO [31]. The formation of FeCr$_2$O$_4$@ZnO@MgO nanoparticles has shown in Fig.1(c). The peak at 580 cm^{-1} is assigned to the Mg-O stretching vibration in Mg (OH)$_2$. The absorption peak at 1510 cm^{-1} is due to the bending vibration of the (OH) bond. The peak at 878 cm^{-1} signifies the out-of-plane aromatic stretching of MgO [32].

X-Ray Diffraction Studies (XRD)

XRD analysis, which is the most useful technique for the identification of crystalline structure, was employed to study the obtained sample. The crystalline structure of the as-prepared FeCr$_2$O$_4$ nanostructure was recognized by XRD analysis. Fig. 2(a) indicates that the pattern matches the JCPDS 24-0512 [33] file identifying FeCr$_2$O$_4$. Based on the XRD analysis the crystal structure of
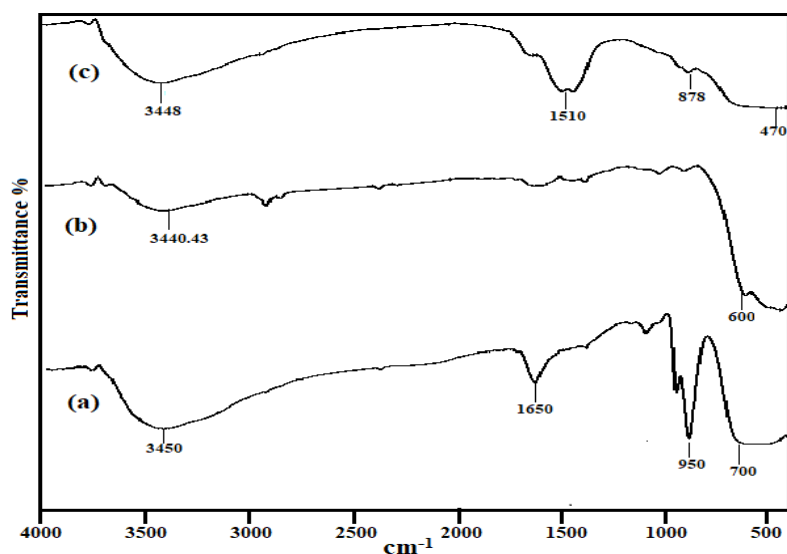
Fig. 1. FTIR spectra of a) FeCr$_2$O$_4$, b) FeCr$_2$O$_4$@ZnO, and c) FeCr$_2$O$_4$@ZnO@MgO
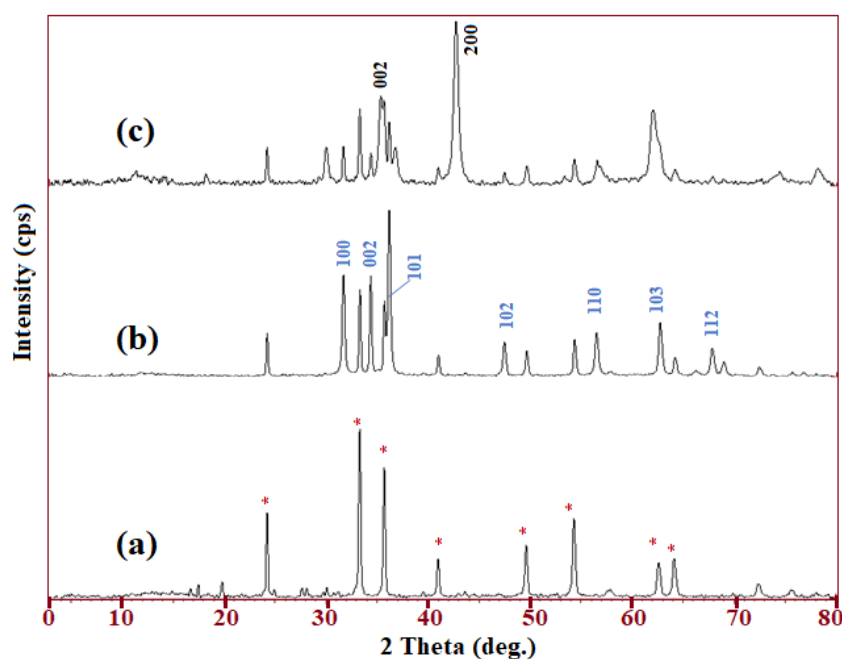
Fig. 2. XRD pattern of a) FeCr$_2$O$_4$, b) FeCr$_2$O$_4$@ZnO, and c) FeCr$_2$O$_4$@ZnO@MgO

the FeCr$_2$O$_4$ is cubic spinel. Fig. 2(b) shows XRD patterns of the products after subsequent thermal decomposition of ZnO in the presence of magnetite cores. Fig. 2(b) depicts the presence of seven new sharp and strong diffraction peaks along with *hkl* planes at 31.90, 34.48, 36.10, 47.35, 56.82, 62.96, and 68.98 were observed.

The position and relative intensity of these new peaks match well with (1 0 0), (0 0 2), (1 0 1), (1 0 2), (1 1 0), (1 0 3), and (1 1 2) planes of the standard data for the hexagonal wurtzite structure of the bulk ZnO (JCPDS file No. 36-1451) [31]. No peaks corresponding to the impurities are detected, indicating that FeCr$_2$O$_4$@ZnO heterostructure was formed during the decomposition process. In the case of FeCr$_2$O$_4$@ZnO@MgO core-shell
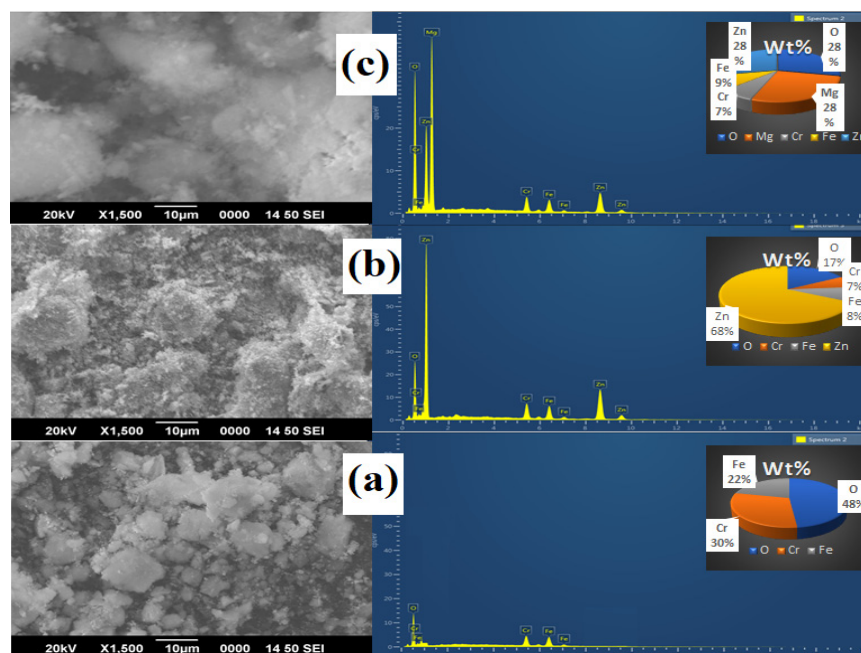
J. Water Environ. Nanotechnol., 6(2): 164-176 Spring 2021

167

Fig. 3. SEM and EDAX analysis of a) FeCr$_2$O$_4$, b) FeCr$_2$O$_4$@ZnO, and c) FeCr$_2$O$_4$@ZnO@MgO

nanoparticles arrays, the XRD pattern, Fig. 2(c) shows the coexistence of ZnO and MgO phases, indicating that MgO was coated on the ZnO nanoparticles. The (0 0 2) strongest diffraction peak appearing in both XRD patterns indicated that the nanoparticles are preferentially oriented in the c-axis direction. Moreover, we can observe that the (0 0 2) peak position slightly shifts from 34.48 to 34.91 due to the MgO coating on the ZnO nanoparticles, and one more new sharp and strongest diffraction peak appear at 42.90 and this new peak matches well with (2 0 0) [34].

Scanning Electron Microscopy (SEM)

The scanning electron microscopy (SEM) image of the FeCr$_2$O$_4$ nanoparticle shows a spongy structure, but the obtained particle size and particle distribution were larger. In order to prove the existence of the elemental analysis EDX analysis was applied. This analysis confirms that the presence of elements in this sample is Fe, Cr, and O only with appropriate proportion Fig. 3(a).

Fig. 3(b) gives the typical SEM image of FeCr$_2$O$_4$@ZnO nanoparticles and gives information on the morphology of the sample prone to aggregation due to the surface area to volume ratio which is spherical and granular for both resolutions. The larger particle size of the

nanostructure was observed flower-shaped and EDX analysis confirms Zn, Fe, Cr, and O elements are present. Fig. 3(c) shows the morphology of FeCr$_2$O$_4$@ZnO@MgO core-shell nanoparticles. Furthermore, to reaffirm the formation of the core-shell nanoparticles EDX analysis data was taken in Fig. 3(c) confirmed the presence of Zn and Mg elements at every point which signifies the coating of MgO on ZnO nanoparticles.

Transmission Electron Microscopy (TEM)

The TEM analysis of FeCr$_2$O$_4$ nanoparticles prepared at 800 ^{0}C is illustrated in Fig. 4(a), These particles possess a regular cubic structure and a uniform width. The surfaces of the cubes were equal and the boundaries of them are evident and the particle size of FeCr$_2$O$_4$ is 98 nm. The SAED pattern in Fig. 4(a), which was parallel to the uprightness axis of the cube surface, indicates that the cubes were single crystalline. Fig. 4(b) shows representative TEM and SEAD patterns of as-prepared magnetite Cores. After thermal decomposition it is seen that the zinc precursor in the presence of FeCr$_2$O$_4$ cores, layers of ZnO shells were deposited on the surface of magnetite cores, the particle size obtains for FeCr$_2$O$_4$@ZnO is 54 nm. Fig. 4(c) shows the TEM images of the core-shell structured nanoparticles. It can be seen
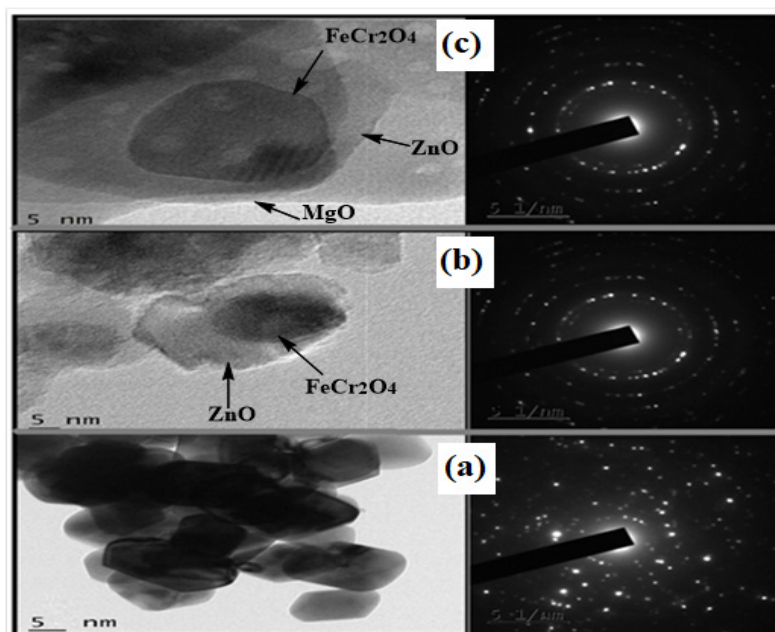
168

J. Water Environ. Nanotechnol., 6(2): 164-176 Spring 2021

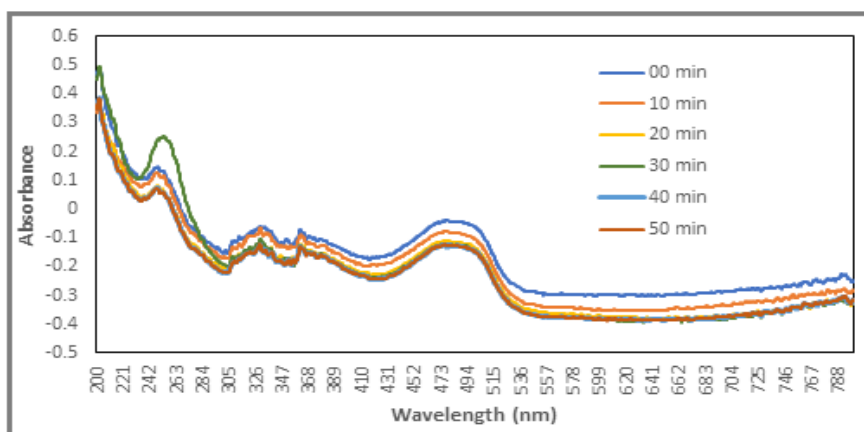Fig. 4. TEM and SEAD analysis of a) $FeCr_2O_4$, b) $FeCr_2O_4$@ZnO, and c) $FeCr_2O_4$@ZnO@MgO

Fig. 5. Graphs showing the dye degradation in presence of $FeCr_2O_4$@ZnO@MgO without UV light.

that the sizes of the resulting nanoparticles while the resulting nanoparticles still retain their spheral morphology. The particle size of synthesized $FeCr_2O_4$@ZnO@MgO nanoparticle is 23nm. From a higher resolution TEM image, the core-shell structure of the particles can be identified. This indicated that MgO is selectively deposited on the $FeCr_2O_4$@ZnO cores instead of homogeneous nucleation and growth in solution.

Photocatalytic Activity of Synthesized Nanoparticles

The photocatalytic property of $FeCr_2O_4$@ZnO@MgO core-shell nanoparticles was investigated

by the photodegradation of Orange G dye. The photodegradation of dye was studied by measuring the absorbance every 10 min using a double beam spectrophotometer. The photodegradation of Orange G dye 10 ppm using $FeCr_2O_4$@ZnO@MgO core-shell 0.5 g nanoparticles as photocatalyst. Fig. 5 indicates there is no effect on absorbance in presence of $FeCr_2O_4$@ZnO@MgO core-shell nanoparticles in dark and absence of UV-Visible light, respectively.

In the next experiment very small change in absorbance is recorded when dye solution 10 ppm was irradiated under visible light in the absence
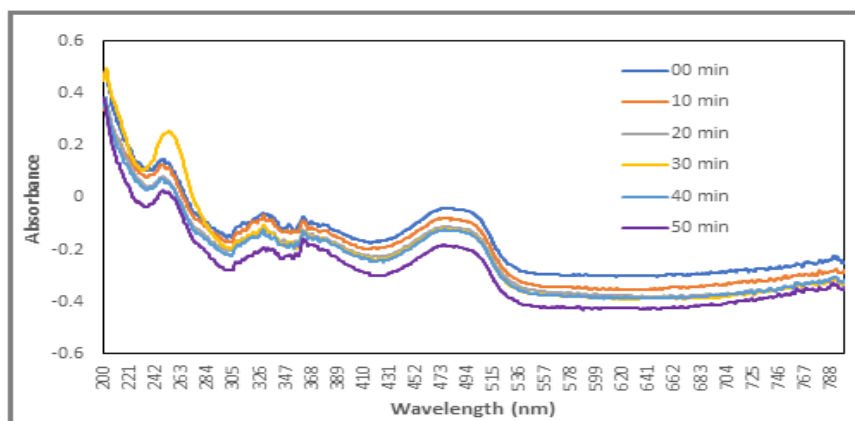
J. Water Environ. Nanotechnol., 6(2): 164-176 Spring 2021

169

Fig. 6. Graphs showing the dye degradation without FeCr$_2$O$_4$@ZnO@MgO with UV light.
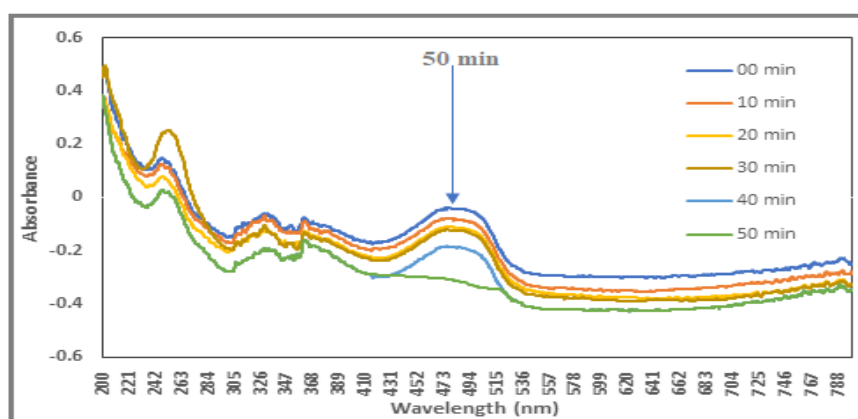

Fig. 7. Graphs showing the dye degradation in presence of FeCr$_2$O$_4$@ZnO@MgO Core-shell nanoparticles with UV light.

of FeCr$_2$O$_4$@ZnO@MgO core-shell Nanoparticles (Fig.6). Fig. 7 reveals the degradation of Orange G dye 10 ppm before and after exposure to the visible light and FeCr$_2$O$_4$@ZnO@MgO core-shell 0.5 g nanoparticles as a Photocatalyst. It is observed that with increasing time of irradiation, this increase in degradation may be due to an increase in the ejection of the number of photons and electrons in the conduction band and the valence band, respectively. The chromophoric absorption peak at 475 nm could be assigned to the n-π* transition of the -N=N- group [35-37]. During the degradation process, the dark colorization in the Orange G dye solution was completely diminished. The color of the solution (absorbance 475 nm) decreased remarkably reaching a discoloration. This shows that the chromophore and conjugated system were being destroyed. Fig. 7 confirms that within 50 min the absorbance peak in the presence of FeCr$_2$O$_4$@

ZnO@MgO core-shell nanoparticles is completely diminished.

Effect of Dye Concentration

The photocatalytic degradation of Orange G dye with various concentrations (10 to 50 ppm) was studied with the stacking of 0.2 g FeCr$_2$O$_4$@ZnO@MgO core-shell nanoparticles in 100 ml dye solution. Fig. 8 shows that when the concentration of Orange G dye increases, the degradation efficiency of the dye decreases gradually. It was suggested that at a lower concentration of the dye, the photocatalytic response rate is around relative to the dye concentration.

Effect of Amount of Catalyst

To examine the photocatalytic degradation of Orange G dye, the streamlining of photocatalyst is a significant factor. Fig. 9 shows the variation in
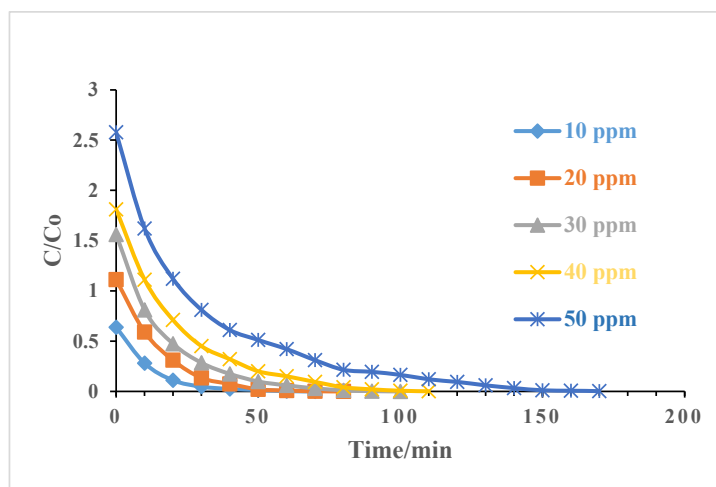
170

J. Water Environ. Nanotechnol., 6(2): 164-176 Spring 2021

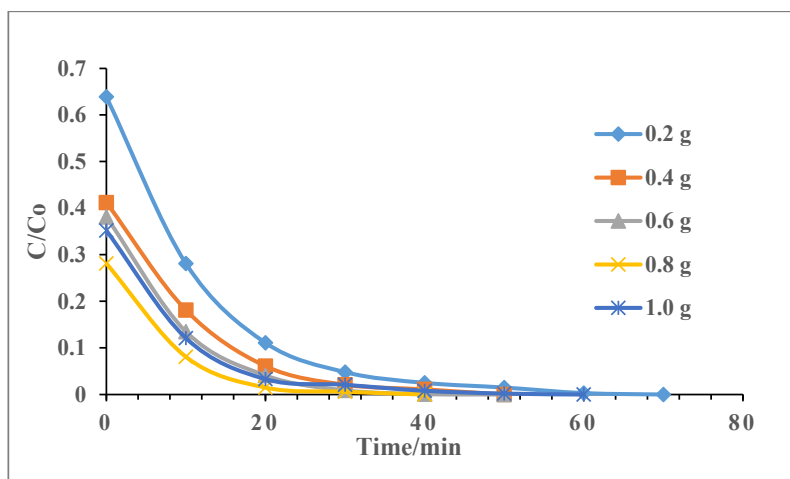Fig. 8. Effect of dye solution on degradation using FeCr$_2$O$_4$@ZnO@MgO core-shell nanoparticles.

Fig. 9. Effect of amount of FeCr$_2$O$_4$@ZnO@MgO Core-Shell nanoparticles on dye degradation.

the amount of Photocatalyst (0.2 to 1.0 g) with 10 ppm dye solution in the presence of UV or visible light. As the amount of Photocatalyst increases, the degradation efficiency increases up to 0.8 g of catalyst, further the increase in the amount of catalyst decreases the photodegradation. Because the photons are get scattered on excess addition of photocatalyst from its surface and hence degradation rate decreases [38]. Fig. 9 affirms that within 50 min the absorbance reaches a minimum in the presence of 0.8 g FeCr$_2$O$_4$@ZnO@MgO core-shell nanoparticles.

Effect of Electrolytes

The presence of inorganic anions like chloride, sulfate, carbonate, nitrate, and phosphate are

impressively basic in wastewaters and normal water. The significance of anions' impact on the photodegradation of pollutants has been remarkably recognized due to the occurrence of the competitive adsorption, resulting in the inhibitive effect on the photoreaction of organic pollutants. Fig. 10 shows the effects of different anions (i.e. Cl^-, SO_4^{-2}, HCO_3^-, NO_3^- and PO_4^{-3}) at the same concentration of 0.05 M. Compared to the without anion test in the aqueous Orange G dye solutions, the existence of all anions reduced the dye degradation to a certain degree.

Among them, the strongest inhibition of Orange G dye degradation resulted from HCO_3^- due to its ionic properties, as like SO_4^{-2}, HCO_3^- can inhibit the photodegradation of the Orange G dye
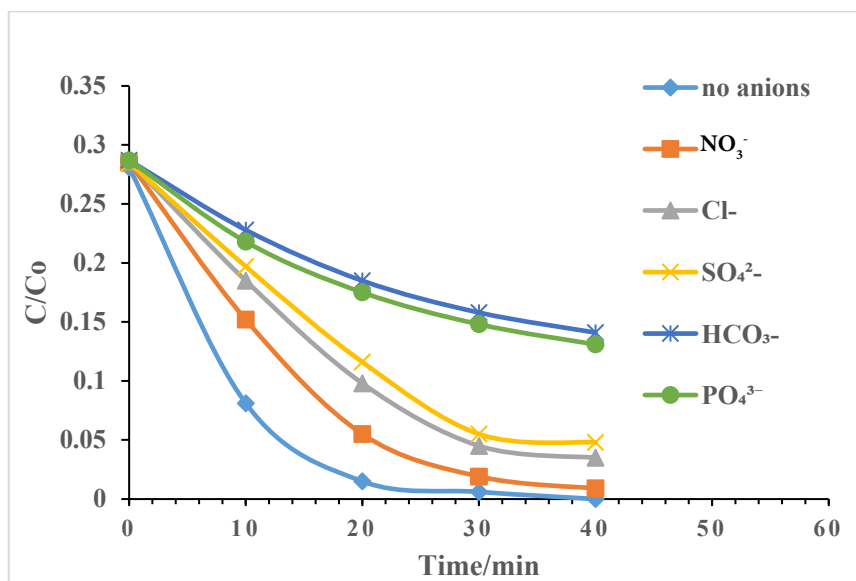
Fig. 10. Effect of Electrolyte for degradation of Orange G dye in presence of FeCr$_2$O$_4$@ZnO@MgO

through competitive adsorption with the Orange G dye on the catalyst surface due to the higher ionic strength and trapping positive holes (h$^+$) and hydroxyl radical (·OH), where HCO$_3^-$ can be led to the generation of less reactive radical HCO$_3^·$. The divalence charge of HCO$_3^-$ can lead to the stronger binding of the HCO$_3^-$ with the photocatalyst, as compared with the single valence ions such as Cl$^-$, and PO$_4^{-3}$, thus resulting in the stronger competitive adsorption. For the addition of PO$_4^{-3}$, the behavior of PO$_4^{-3}$ ions is similar to HCO$_3^-$ ions, in that the PO$_4^{-3}$ reacted with h$^+$ and ·OH to form PO$_4^{-3}$, less reactive than that of h$^+$ and ·OH. The formation of inorganic radical anions under these circumstances was also reported in some literature [39,40]. The addition of NO$_3^-$ to the Orange G dye solution in this study showed a minor effect on the photocatalytic degradation of Orange G dye only. The presence of NO$_3^-$ had a negligible effect on the photodegradation of Orange G dye under UV light irradiation, the observed inhibition effect may be therefore explained by the combination of the competitive adsorption and the formation of less reactive radicals during the photocatalytic reactions.
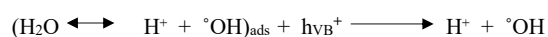
Degradation Mechanism of Orange G dye

The photocatalytic degradation mechanism for Orange G dye in presence of core-shell FeCr$_2$O$_4$@ZnO@MgO is given below
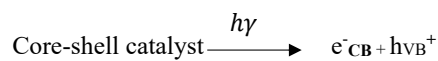
Core-shell catalyst $\xrightarrow{h\gamma}$ e$^-$$_{CB}$ + h$_{VB}^+$

Oxygen ion absorption

(O$_2$)$_{ads}$ + e$^-$$_{CB}$ $\longrightarrow$ O$_2^-$
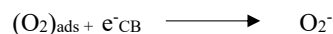
Neutralization of $^-$OH group into ·OH radical by photo holes.

(H$_2$O $\longleftrightarrow$ H$^+$ + ·OH)$_{ads}$ + h$_{VB}^+$ $\longrightarrow$ H$^+$ + ·OH

Oxidation of Orange G dye via successive attacks by ·OH radicals.

R + h$_{VB}^+$ $\longrightarrow$ ·R + H$_2$O

or by direct reaction with holes

R + h$_{VB}^+$ $\longrightarrow$ R$^+$ $\longrightarrow$ degraded products

Lastly, holes react directly with carboxylic acid, producing CO$_2$ by the photo-Kolbe process.

·OH + RH $\longrightarrow$ H$_2$O + ·R

·R + O$_2$ $\longrightarrow$ ROO· $\longrightarrow$ CO$_2$
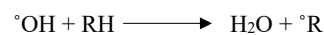
Compare Photocatalytic Efficiency of Synthesised Nanoparticles

Efficiency checks the synthesized photocatalyst, the photocatalytic degradation checked by the same concentration of Orange G dye (10 ppm) by loading same amount (0.8g) of synthesized photocatalyst in

Fig. 11. Compare Photocatalytic Efficiency of Synthesised nanoparticles.

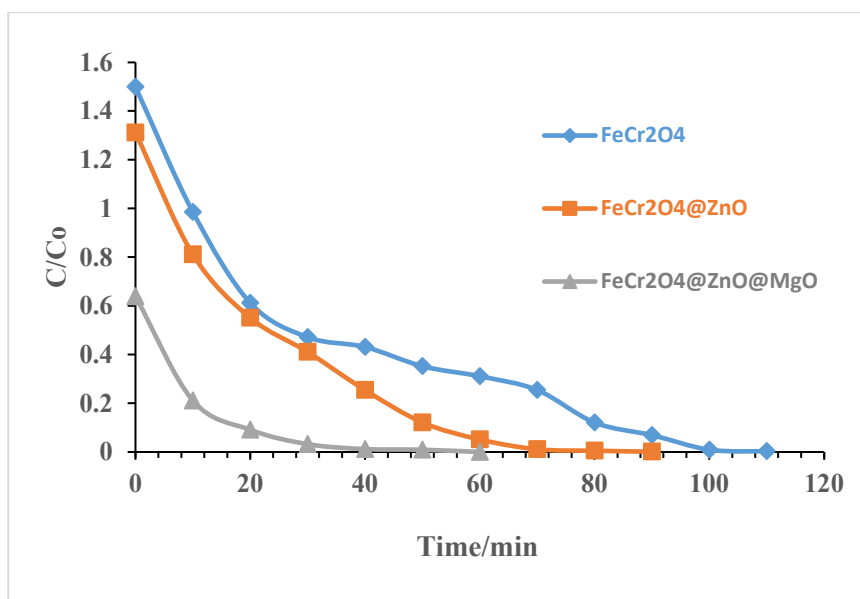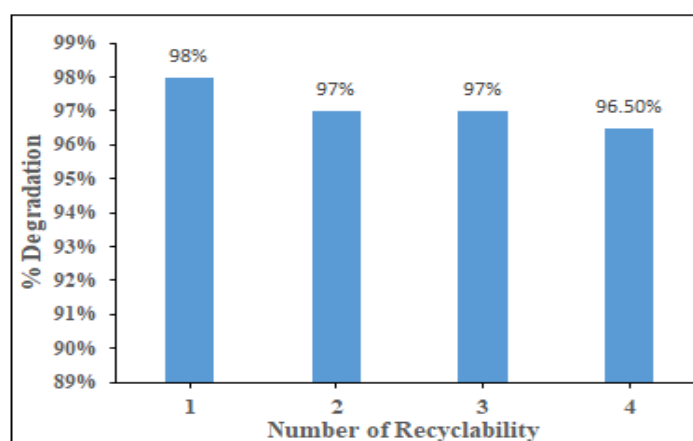Fig. 12. Recyclability of FeCr$_2$O$_4$@ZnO@MgO Core-Shell nanoparticles for degradation of Orange G dye.

100 ml Orange G dye solution.

Fig. 11 shows that the rapid degradation of dye in presence of synthesized FeCr$_2$O$_4$@ZnO@MgO core-Shell nanoparticles as a photocatalyst is more efficient than FeCr$_2$O$_4$@ZnO and FeCr$_2$O$_4$ nanoparticles. In comparison, the rate of Orange G dye degradation is faster in presence of FeCr$_2$O$_4$@ZnO@MgO because ZnO and MgO coating catalyzing the photo-oxidation process of the dye molecule faster. Further, it is also concluded that the particle size of FeCr$_2$O$_4$@ZnO@MgO is smaller as compared to other products and hence the surface area is more for faster degradation.

Recyclability of Photocatalyst

Degradation of Orange G dye Fig. 12 shows the recyclability of FeCr$_2$O$_4$@ZnO@MgO Core-Shell nanoparticles for the degradation of Orange G dye. After every run, this photocatalyst was separated from dye solution using the centrifugation method, washed with distilled water, dried at 150 ^{0}C in an oven and calcined at 600 ^{0}C in a muffle furnace for removing organic matter, and this activated photocatalyst was redistributed in fresh Orange G dye solution. We observed that in each run the extent of catalyst loss may cause a decrease in degradation.
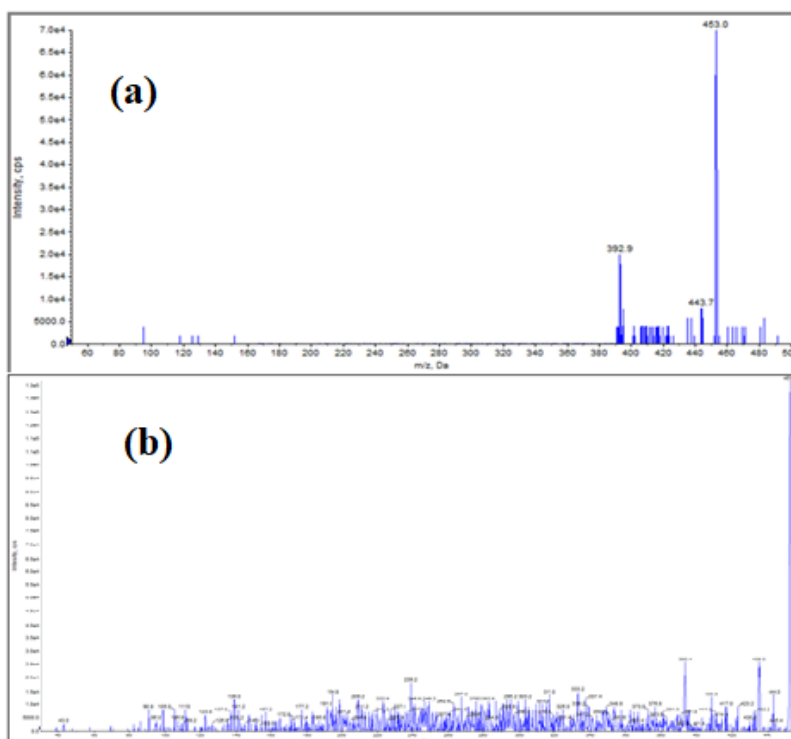
Fig. 13. LC-MS of (a) Before degradation of Orange G dye, (b) After degradation of Orange G dye.
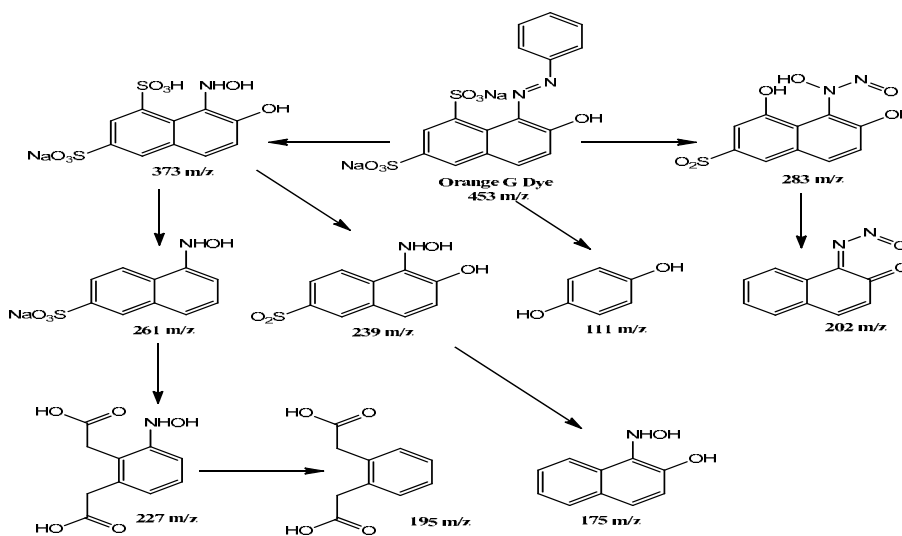
Fig. 14. Degradation mechanism of Orange G dye.

LC-MS OF DEGRADED ORANGE G DYE

The mechanism for the degradation of Orange G dye was established by using liquid chromatography-mass spectroscopy (LC-MS). The LC-MS recorded before degradation is shown in Fig. 13(a). A broad peak of Orange G dye was observed at 453 m/z, and completely degraded Orange G dye is shown in Fig. 13(b). The Orange G dye degradation pathway is represented in Fig. 14. The structure of different products was suggested based on HPLC–MS fragmentation. In the present molecule, peaks of Orange G dye were observed at 461 m/z; before irradiation, only parent dye is present as expected. There are several fragments at

174

J. Water Environ. Nanotechnol., 6(2): 164-176 Spring 2021

373 m/z, 283 m/z, 261 m/z, 239 m/z, 227 m/z, 202 m/z, 195 m/z, 175 m/z, and 111 m/z that occur after the degradation of Orange G dye.

CONCLUSIONS

In the present investigation, normal spinel nanocrystalline pure Iron (II) chromite coated with Zinc oxide and Magnesium oxide core-shell has been synthesized by the sol-gel method. Synthesis of $FeCr_2O_4$@ZnO@MgO core-shell nanoparticles confirmed through FT-IR, XRD, SEM-EDX, and HR-TEM-SAED analysis. Synthesized $FeCr_2O_4$@ZnO@MgO core-shell nanoparticles were found to be a better photocatalyst in UV light for the degradation of Orange G dye. Orange G dye solutions of lower concentration were completely mineralized by Photocatalyst under UV light irradiation. The degraded products were analyzed using liquid chromatography-mass spectroscopy (LCMS). The analysis revealed that the photocatalytic degradation of the Orange G dye molecule resulted in the formation of intermediate products such as substituted aromatic hydroxylamine, nitroso, and phenol compounds. The highest degradation of Orange G dye was found at 0.8 g $FeCr_2O_4$@ZnO@MgO, 10 ppm Orange G dye, and the time required is only 50 min.

CONFLICTS OF INTEREST

The authors declare there are no conflicts of interest.

REFERENCES

1. Jamshidi M, Ghaedi M, Dashtian K, Hajati S. New ion-imprinted polymer-functionalized mesoporous SBA-15 for selective separation and preconcentration of Cr(iii) ions: modeling and optimization. RSC Advances. 2015;5(128):105789-99.
2. Gupta VK, Saleh TA. Sorption of pollutants by porous carbon, carbon nanotubes and fullerene- An overview. Environmental Science and Pollution Research. 2013;20(5):2828-43.
3. Mazaheri H, Ghaedi M, Hajati S, Dashtian K, Purkait MK. Simultaneous removal of methylene blue and Pb2+ ions using ruthenium nanoparticle-loaded activated carbon: response surface methodology. RSC Advances. 2015;5(101):83427-35.
4. Gupta VK, Jain R, Mittal A, Saleh TA, Nayak A, Agarwal S, et al. Photo-catalytic degradation of toxic dye amaranth on TiO2/UV in aqueous suspensions. Materials Science and Engineering: C. 2012;32(1):12-7.
5. Baleizao. C., Gigante. B., Garcia. H., Corma. A. Ionic liquids as green solvents for themasymmetric synthesis of cyanohydrins catalysed by VO (salen) complexes. Green Chem. 2002;(**4**) :272–274.
6. Colvin VL. The potential environmental impact of engineered nanomaterials. Nature Biotechnology. 2003;21(10):1166-70.
7. Hurt RH, Monthioux M, Kane A. Toxicology of carbon nanomaterials: Status, trends, and perspectives on the special issue. Carbon. 2006;44(6):1028-33.
8. Subramanian V, Zhu H, Vajtai R, Ajayan PM, Wei B. Hydrothermal Synthesis and Pseudocapacitance Properties of MnO2Nanostructures. The Journal of Physical Chemistry B. 2005;109(43):20207-14.
9. Lorimer JP, Mason TJ, Plattes M, Phull SS, Walton DJ. Degradation of dye effluent. Pure and Applied Chemistry. 2001;73(12):1957-68.
10. Borhade A, Tope D, Kushare S. Mercenaria Shell Powder as a Cost-Effective and Eco-friendly Photocatalyst for the Degradation of Eriochrome Black T Dye. Iranian Journal of Science and Technology, Transactions A: Science. 2019;44(1):75-83.
11. Pinheiro HM, Touraud E, Thomas O. Aromatic amines from azo dye reduction: status review with emphasis on direct UV spectrophotometric detection in textile industry wastewaters. Dyes and Pigments. 2004;61(2):121-39.
12. Xie YB, Li XZ. Interactive oxidation of photoelectrocatalysis and electro-Fenton for azo dye degradation using TiO2–Ti mesh and reticulated vitreous carbon electrodes. Materials Chemistry and Physics. 2006;95(1):39-50.
13. Zhiyong Y, Keppner H, Laub D, Mielczarski E, Mielczarski J, Kiwi-Minsker L, et al. Photocatalytic discoloration of Methyl Orange on innovative parylene–TiO2 flexible thin films under simulated sunlight. Applied Catalysis B: Environmental. 2008;79(1):63-71.
14. Bettinelli M, Dallacasa V, Falcomer D, Fornasiero P, Gombac V, Montini T, et al. Photocatalytic activity of TiO2 doped with boron and vanadium. Journal of Hazardous Materials. 2007;146(3):529-34.
15. Bahnemann DW. Mechanisms of Organic Transformations on Semiconductor Particles. Photochemical Conversion and Storage of Solar Energy: Springer Netherlands; 1991. p. 251-76.
16. Okamoto K-i, Yamamoto Y, Tanaka H, Tanaka M, Itaya A. Heterogeneous Photocatalytic Decomposition of Phenol over TiO2Powder. Bulletin of the Chemical Society of Japan. 1985;58(7):2015-22.
17. Sharma A, Rao P, Mathur RP, Ameta SC. Photocatalytic reactions of xylidine ponceau on semiconducting zinc oxide powder. Journal of Photochemistry and Photobiology A: Chemistry. 1995;86(1-3):197-200.
18. Gupta VK, Gupta B, Rastogi A, Agarwal S, Nayak A. A comparative investigation on adsorption performances of mesoporous activated carbon prepared from waste rubber tire and activated carbon for a hazardous azo dye—Acid Blue 113. Journal of Hazardous Materials. 2011;186(1):891-901.
19. Gupta VK, Jain R, Nayak A, Agarwal S, Shrivastava M. Removal of the hazardous dye—Tartrazine by photodegradation on titanium dioxide surface. Materials Science and Engineering: C. 2011;31(5):1062-7.
20. Gupta VK, Jain R, Mittal A, Saleh TA, Nayak A, Agarwal S, et al. Photo-catalytic degradation of toxic dye amaranth on TiO2/UV in aqueous suspensions. Materials Science and Engineering: C. 2012;32(1):12-7.
21. Reeves P, Ohlhausen R, Sloan D, Pamplin K, Scoggins T, Clark C, et al. Photocatalytic destruction of organic dyes in aqueous TiO2 suspensions using concentrated simulated

J. Water Environ. Nanotechnol., 6(2): 164-176 Spring 2021

175

and natural solar energy. Solar Energy. 1992;48(6):413-20.

22. Khodja AA, Sehili T, Pilichowski J-F, Boule P. Photocatalytic degradation of 2-phenylphenol on TiO2 and ZnO in aqueous suspensions. Journal of Photochemistry and Photobiology A: Chemistry. 2001;141(2-3):231-9.

23. Yatmaz HC, Akyol A, Bayramoglu M. Kinetics of the Photocatalytic Decolorization of an Azo Reactive Dye in Aqueous ZnO Suspensions. Industrial & Engineering Chemistry Research. 2004;43(19):6035-9.

24. Serpone N, Maruthamuthu P, Pichat P, Pelizzetti E, Hidaka H. Exploiting the interparticle electron transfer process in the photocatalysed oxidation of phenol, 2-chlorophenol and pentachlorophenol: chemical evidence for electron and hole transfer between coupled semiconductors. Journal of Photochemistry and Photobiology A: Chemistry. 1995;85(3):247-55.

25. Wei S, Wang Q, Zhu J, Sun L, Lin H, Guo Z. Multifunctional composite core–shell nanoparticles. Nanoscale. 2011;3(11):4474.

26. Chen X, Dobson PJ. Synthesis of Semiconductor Nanoparticles. Nanoparticles in Biology and Medicine: Humana Press; 2012. p. 103-23.

27. Clime L, Drogoff BL, Zhao S, Zhang Z, Veres T. Magnetic nanocarriers: from material design to magnetic manipulation. International Journal of Nanotechnology. 2008;5(9/10/11/12):1268.

28. Corr SA, Rakovich YP, Gun'ko YK. Multifunctional Magnetic-fluorescent Nanocomposites for Biomedical Applications. Nanoscale Research Letters. 2008;3(3):87-104.

29. Xu. B., Wu. K., Chen. Z. Tribology properties of CuS nanoparticals In-situ synthesized in liquid paraffin. Guangzhou Chem. Ind. 2010;(**38**): 147–149.

30. Wan J, Li H, Chen K. Synthesis and characterization of Fe3O4@ZnO core–shell structured nanoparticles. Materials Chemistry and Physics. 2009;114(1):30-2.

31. Ramachandran T, Hamed F. The effect of fuel to nitrates ratio on the properties of FeCr2O4 nanopowders. Materials Research Bulletin. 2017;95:104-14.

32. Vijayaprasath G, Murugan R, Asaithambi S, Sakthivel P, Mahalingam T, Hayakawa Y, et al. Structural and magnetic behavior of Ni/Mn co-doped ZnO nanoparticles prepared by co-precipitation method. Ceramics International. 2016;42(2):2836-45.

33. Sharifi SH, Shoja H. Optimization of process variables by response surface methodology for methylene blue dye removal using Spruce sawdust/MgO nano-biocomposite. J. Water Environ. Nanotechnol., 2018; **3(2):** 157-172.

34. Abbasi A., Keihan AH., Ahmadi Golsefidi M., Rahimi-Nasrabadi M., Khojasteh H. Synthesis, Characterization and Photocatalytic Activity of FeCr2 O4 and FeCr2 O4 /Ag Nanocomposites. J Nanostruct, 2020; **10(3):** 518-530

35. Zhao X, Yang H, Wu P, Huang X, Wang X. The preparation of MgO nanopowders synthesized via an improved polyacrylamide gel method. RSC Advances. 2019;9(26):14893-8.

36. Xu X-R, Li X-Z. Degradation of azo dye Orange G in aqueous solutions by persulfate with ferrous ion. Separation and Purification Technology. 2010;72(1):105-11.

37. Ou X, Yan J, Zhang F, Zhang C. Accelerated degradation of orange G over a wide pH range in the presence of FeVO4. Frontiers of Environmental Science & Engineering. 2018;12(1).

38. Muthukumar M, Karuppiah MT, Raju GB. Electrochemical removal of CI Acid orange 10 from aqueous solutions. Separation and Purification Technology. 2007;55(2):198-205.

39. Mahlambi MM, Ngila CJ, Mamba BB. Recent Developments in Environmental Photocatalytic Degradation of Organic Pollutants: The Case of Titanium Dioxide Nanoparticles—A Review. Journal of Nanomaterials. 2015;2015:1-29.

40. Abdullah M, Low GKC, Matthews RW. Effects of common inorganic anions on rates of photocatalytic oxidation of organic carbon over illuminated titanium dioxide. The Journal of Physical Chemistry. 1990;94(17):6820-5.

41. Bekbölet M, Boyacioglu Z, özkaraova B. The influence of solution matrix on the photocatalytic removal of color from natural waters. Water Science and Technology. 1998;38(6):155-62.

176

J. Water Environ. Nanotechnol., 6(2): 164-176 Spring 2021